Carbohydrate Polymers 87 (2012) 1026–1037

Contents lists available at ScienceDirect

Carbohydrate Polymers

journal homepage: www.elsevier.com/locate/carbpol

Surface area and porosity of acid hydrolyzed cellulose nanowhiskers and cellulose produced by *Gluconacetobacter xylinus*

Jing Guo[a,c], Jeffrey M. Catchmark[a,b,c,*]

[a] Intercollege Graduate Degree Program in Plant Biology, The Pennsylvania State University, University Park, PA 16802, USA
[b] Department of Agricultural and Biological Engineering, The Pennsylvania State University, University Park, PA 16802, USA
[c] Center for NanoCellulosics, The Pennsylvania State University, University Park, PA 16802, USA

ARTICLE INFO

Article history:
Received 16 April 2011
Received in revised form 21 July 2011
Accepted 26 July 2011
Available online 10 August 2011

Keywords:
Cellulose nanowhiskers
Acid hydrolysis
Bacterial cellulose
Surface area
Porosity

ABSTRACT

The physical parameters of cellulose such as surface area and porosity are important in the development of cellulose composites which may contain valuable additives which bind to cellulose. In this area, the use of acid hydrolyzed nano-dimensional cellulose nanowhiskers (CNWs) has attracted significant interest, yet the surface area and porosity of these materials have not been explored experimentally. The objective of this work was to characterize the surface area and porosity of CNWs from different origins (plant cotton/bacterium *Gluconacetobacter xylinus*) and different acid treatments (H_2SO_4/HCl) by N_2 adsorption; as well as to compare surface area and porosity of bacterial cellulose synthesized by static and agitated cultures. Our results showed that CNWs produced from H_2SO_4/HCl exhibited significantly increased surface area and porosity relative to starting material cotton fiber CF11. Micropores were generated in HCl hydrolyzed CNWs but not in H_2SO_4 hydrolyzed CNWs. Bacterial CNWs exhibited larger surface area and porosity compared to plant CNWs. Cellulose synthesized by *G. xylinus* ATCC 700178 from agitated cultures also exhibited less surface area and porosity than those from static cultures.

1. Introduction

Cellulose is a high molecular weight polymer comprised of D-glucopyranosyl units but is complicated due to different packing and aggregation of cellulose chains, which varies among cellulose producing organisms, yielding a heterogeneous and porous structure. It is believed that the shape of an elementary fibril is determined by the cellulose synthase as well as by the local environment in which the cellulose is produced (Doblin, Kurek, Jacob-Wilk, & Delmer, 2002). In plants, cellulose is produced by a rosette (Brown & Montezinos, 1976), which produces a number of individual glucan chains which crystallize into an elementary fibril. Multiple elementary fibrils will subsequently aggregate into larger bundles. It has been suggested that pores may be present in the amorphous regions, which may exist as periodic defects along the cellulose fibril (Nishiyama et al., 2003). The aggregation of elementary fibrils into bundles has also been cited as a source of porosity (Delmer & Amor, 1995). It was found that cotton cellulose had pores ~4–5 nm in diameter, with a crystallite of 4–5 nm in width (Aggebrandt & Samuelson, 1964; Klemm, Heublein, Fink, & Bohn, 2005; Morosoff, 1974), while wood cellulose crystallites have been determined to have widths of ~3.5–4 nm (Ioelovitch, 1992). Compared to plant cellulose, in which cellulose Iβ is the major component, bacterial cellulose (e.g., bacterium *Gluconacetobacter xylinus*, a well characterized cellulose producer) is predominantly cellulose Iα (Attala & Vanderhart, 1984). Bacterial cellulose has a unique structure, which is almost pure without any lignin or hemicellulose. Moreover, bacterial cellulose possesses higher surface area compared to plant cellulose (Krieger, 1990; Sakairi, Asano, Ogawa, Nishi, & Tokura, 1998) mainly due to the reduced fiber diameter and open network structure. It has been proposed that bacterial cellulose has crystallinity of ~75% (Kulshreshtha & Dweltz, 1973), and its crystallites are ~5–6 nm in width (Klemm et al., 2005). It is known that different origins and treatments are responsible for the complexity and variability of cellulose structures. Knowledge of surface area and porosity are important in understanding the structure, formation and degradation of cellulose from different origins and treatments. Understanding the surface structure and porosity of cellulose is fundamental to its use as a feedstock for biofuels. For example, previous work suggested that the surface area of cellulose was of particular significance in affecting enzymatic cellulose hydrolysis (Fan, Lee, & Beardmore, 1981) because the direct physical contact between cellulases and the surface of cellulose determined the accessibility of the cellulases to cellulose, which was a prerequisite to hydrolysis (Thompson, Chen, & Grethlein, 1992). High surface area and pore

* Corresponding author at: Intercollege Graduate Degree Program in Plant Biology, The Pennsylvania State University, University Park, PA 16802, USA.
Tel.: +1 814 863 0414; fax: +1 814 863 1031.
E-mail address: jcatchmark@engr.psu.edu (J.M. Catchmark).

0144-8617/$ – see front matter © 2011 Elsevier Ltd. All rights reserved.
doi:10.1016/j.carbpol.2011.07.060

volume guarantee sufficient adsorption of the cellulases to the cellulose surface. In this area, cellulose nanowhiskers (CNWs) are a subject of intense investigation due to their exceptional physical and mechanical properties, size, availability, and ability to be functionalized with specific surface chemistries through a variety of chemical processes (De Souza Lima & Borsali, 2004; Habibi, Lucia, & Rojas, 2010; Samir, Alloin, & Dufresne, 2005). To date, however, a comprehensive study of the surface area and porosity of acid hydrolyzed CNWs has not been performed experimentally.

Numerous methods have been developed and applied for characterizing surface area and porosity of cellulose, e.g., N_2 adsorption, probes (e.g., bovine serum albumin (BSA), peroxidase, etc.) and solute exclusion methods. However, by using probes, a specific surface area of 0.08 m^2/g of Avicel PH101 has been shown, different from that predicted by the N_2 adsorption (2.07 m^2/g) or by cellulase adsorption method (2.5 m^2/g) (Gama, Teixeira, & Mota, 1994). This results from the limitation of using probes, which are highly affected not only by the surface characteristics of cellulose but also by their specific adsorption affinities. On the other hand, solute exclusion method also exhibits several disadvantages: (1) the measured pore volume and area are largely dependent on the probe size, i.e., the pores not accessible to probes of certain sizes may not be evaluated; only the internal pore surface can be estimated, the external surface cannot be determined; (2) when measured in solution, cellulose may swell due to the penetration of water into the fibrils, which may overestimate the porosity by pore enlargement; and (3) an inaccurate estimation may also rise from the competition of water to solute probes (Burns, Ooshima, & Converse, 1989). However, the pore size determined by N_2 adsorption is from approximately 0.4 nm to 300 nm (Allen, 1997), a range not covered by most other methods.

Several studies have been performed on the surface area of cellulose materials using the N_2 adsorption method, which show discrepancies in the range of 0.58–200 m^2/g (Papadopoulos, Hill, Gkaraveli, Ntalos, & Karastergiou, 2003; Stone, Scallan, Donefer, & Ahlgren, 1969; Thode, Swanson, & Becher, 1958; Wong, Deverell, Mackie, Clark, & Donaldson, 1988). These discrepancies suggest a dependence of the surface area on sample selection, pretreatment and drying method. In this work, we evaluated the surface area and porosity characteristics of a number of relevant celluloses purified using the most commonly implemented methods. By consistent sample preparation and N_2 adsorption procedure, various cellulose samples treated by different acids and from different origins were able to be compared. The scope of this study is to describe how acid hydrolysis and origins influence the microstructure of cellulose.

2. Materials and methods

2.1. Cellulose samples

Avicel PH101 microcrystalline cellulose, extracted from wood pulp, was purchased from Sigma–Aldrich. Whatman™ CF11 cellulose powder (cotton origin) was purchased from Whatman International Ltd. The cellulose nanowhiskers (CNWs) were produced from Whatman™ CF11 cellulose by sulfuric acid (63.5%, w/w) according to the procedures implemented by Bondeson, Mathew, and Oksman (2006; Marchessault, Morehead, & Walter, 1959; Marchessault, Morehead, & Koch, 1961). 55 g cellulose was added into 1 L of 0.1 M NaOH solution with stirring for 1–2 h, followed by several washing steps to eliminate residual NaOH. The washed cellulose was then added into 500 ml of sulfuric acid (63.5%, w/w), the hydrolysis was carried out under 45 °C with continuous stirring for 90 min and further hydrolysis was stopped by additional washing with deionized (DI) water, after which the pH was neutralized by dialysis with DI water and CNW suspension was obtained after sonication. The HCl treated CNWs were generated from either Whatman™ CF11 (cotton) or *G. xylinus* cellulose by hydrochloric acid (15%, w/w). The hydrolysis parameters were taken from Araki, Wada, Kuga, and Okano (1998). The HCl treated CNW suspension was prepared by treating 5 g of cellulose with 175 ml of 4 N HCl at 80 °C for 225 min. The sediment was collected after several centrifugations, and then purified by dialysis and sonication. After hydrolysis, the solution contained both cellulose particles in the upper fraction of suspension and sediments which accumulated in the lower fraction of the container. In this work, the upper fraction of the solution refers to the smaller suspended CNWs while the lower fraction of the solution refers to the larger sediments. Cellulose films were generated from *G. xylinus* strain ATCC 700178 statically or under agitation in Hestrin–Schramm (HS) medium at 30 °C for 7 days (Hestrin & Schramm, 1954). Freeze-drying method was used for cellulose sample preparation as this process limits the deformation of the polymer during removal of the solvent (Galle, 2001; Ratti, 2001). Especially, the shrinkage of pore structure will be to a large degree prevented at low temperature (Krokida, Karathanos, & Maroulis, 1998). All the cellulose samples were first frozen at −80 °C. This low temperature prevents the growth of big ice crystals that form in larger pores. After freezing, samples were freeze-dried (−40 °C, 0.035 mbar, under such pressure cellulose nanostructure will not be affected) as powders for N_2 adsorption measurements.

2.2. N_2 adsorption measurements

The N_2 adsorption measurements were carried out at 77 K using an Accelerated Surface Area and Porosimetry Analyzer (ASAP 2020; Micrometritics Instrument Corp.). The N_2 adsorption technique quantifies the surface area and porosity characteristics by measuring the amount of N_2 adsorbed and desorbed onto a porous solid material over a wide range of relative pressures (P/P_0, where P is the equilibrium pressure and P_0 is the saturation pressure) of 10^{-8}–1.0. The adsorption isotherms obtained from these adsorption measurements allow for the determination of the surface area, pore volume, and pore size distributions (PSDs) (Gregg & Sing, 1982; Lowell & Shields, 1991; Rouquerol, Rouquerol, & Sing, 1999). The specific surface area is calculated based on Brunauer, Emmett and Teller (BET) theory (Brunauer, Emmett, & Teller, 1938) from the linear part of the adsorption isotherm, at pressures $0.05 < P/P_0 < 0.30$. According to the International Union of Pure and Applied Chemistry (IUPAC) standard (Sing et al., 1985), porous materials can be classified into 3 categories: pores <2 nm in diameter are micropores; pores in the range of 2–50 nm are mesopores; and pores >50 nm are macropores. Pores can be open or closed. In this work, characterization of the open pores is of specific interest, since open pores are capable of accommodating cellulases for cellulose hydrolysis, or binding molecules useful for cellulose nanocomposites. The PSDs of meso- and macropores are calculated using classical pore size model developed by Barret, Joyner and Halenda (BJH), based on the Kelvin equation (Barret, Joyner, & Halenda, 1951). The conventional Horvath–Kawazoe (HK) model (Horvath & Kawazoe, 1983) is mainly applied for micropore size calculations. In this work, we applied all three methods for evaluating the surface area and porosity characteristics of various forms of cellulose. All the samples were degassed at 303.15 K for 240–480 min under vacuum at 10 μm Hg prior to the measurements.

2.3. X-ray diffraction measurements

To determine the crystallinity and crystallite size, the X-ray diffraction (XRD) patterns of the cellulose samples were collected on a PANalytical X'Pert Pro MPD (multi-purpose diffractometer) with Cu$K\alpha$ radiation generation. The diffraction intensity was

Table 1
Crystallinity and crystallite size of cellulose samples.

Sample	Crystallinity (%)	Crystallite size (nm)
CF11	78.2 ± 0.4	7.4 ± 0.1
CNW-H_2SO_4	90.5 ± 1.4	6.8 ± 0.1
CNW-HCl	89.3 ± 1.6	6.6 ± 0.1
BC-CNW-HCl	94.5 ± 1.9	5.8 ± 0.0
BC-static	82.2 ± 0.3	6.2 ± 0.0
BC-agitated	71.5 ± 1.3	5.8 ± 0.1

Only the upper fractions of CNWs were measured by XRD. BC represents bacterial cellulose from *G. xylinus* ATCC 700178. BC static and agitated represent the cellulose produced by *G. xylinus* with static and agitated cultures, respectively. The values were obtained from at least triplicates. The crystallite size of cellulose samples was quantitatively evaluated via the width at half-height of maximum intensity of the (2 0 0) diffraction peak.

measured between 2θ of 5–60°. MDI Jade 9 software (Materials Data, Inc., Livermore, CA) was used to process the diffraction patterns and to calculate the crystallinity of cellulose samples. The crystallite size was estimated from the full width at half-maximum intensity (FWHM) of the reflection (2 0 0) using Scherrer equation (Zhang, Xi, Mo, & Jin, 2003).

$$\beta_{hkl} = \frac{K\lambda}{L_{hkl}\cos\theta_{hkl}}$$

where β is the breadth of the peak of a specific phase (*hkl*, (2 0 0) plane in our case), K is a constant that varies with the method of taking the breadth ($K = 0.94$), λ is the wavelength of incident X-rays ($\lambda = 0.15418$ nm), θ is the center angle of the peak, and L is the crystallite length (size).

2.4. Scanning electron microscopy (SEM)

Cellulose samples were freeze-dried as powders or films, fixed onto an aluminum slab with two-sided adhesive carbon tape, and then sputter-coated with gold (thickness ~ 1 nm). A LEO 1530 (GEMINI) field emission scanning electron microscope (FESEM) operating at 2 kV (low voltage was applied to make sure the morphology of cellulose samples would not be affected) was used for cellulose morphology observation.

2.5. Atomic force microscopy (AFM)

A droplet of diluted CNWs was dispensed onto a mica surface and the sample was dried at room temperature overnight with a dust cover. A NanoScope III atomic force microscope (AFM) was used for CNW morphology observation. All scans were performed in air with commercial Si nanoprobe tips. Height and phase images were obtained simultaneously in tapping mode at the fundamental resonance frequency of the cantilever with a scan rate of 0.5–0.8 Hz. The oscillating amplitude was 0.5 V.

3. Results and discussion

3.1. Cellulose crystallinity and crystallite size determined by XRD

XRD was used to investigate the changes of phase structures of cellulose before and after acid treatments. The crystallinity and crystallite size of cellulose samples were quantitatively evaluated via the relative intensity of the (2 0 0) diffraction peak. Our XRD (Table 1) results suggest that the CNWs produced from H_2SO_4 or HCl hydrolysis (from both plant and bacterial origins) have comparable crystallinity, both higher than that of CF11. Conversely, decreased crystallite size is observed in H_2SO_4/HCl hydrolyzed CNWs. This indicates that H_2SO_4/HCl digestion significantly reduces the amorphous content and/or CNW surface glucan

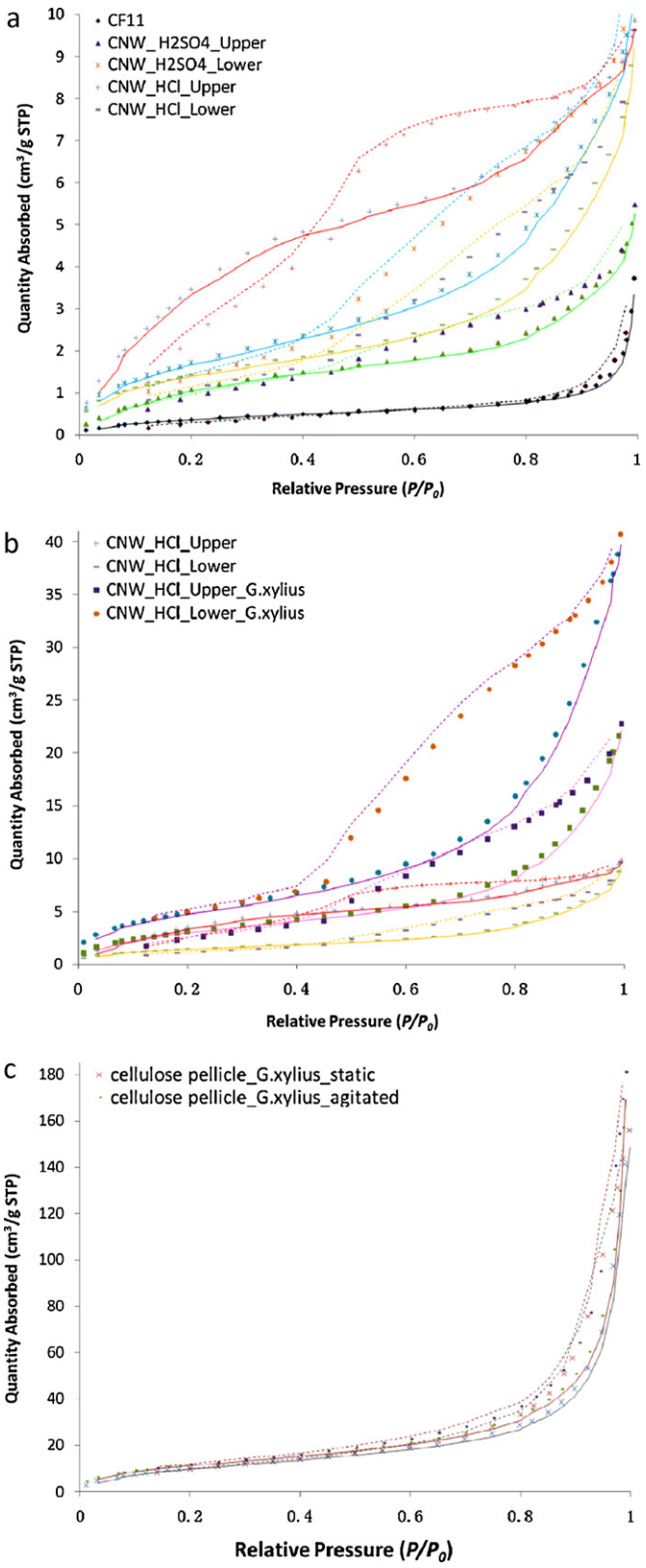

Fig. 1. N_2 adsorption and desorption isotherms of cellulose samples: (a) untreated cotton CF11 and both upper and lower fractions of CNWs prepared from CF11 by H_2SO_4 and HCl hydrolysis; (b) upper and lower fractions of CNWs generated from CF11 and *G. xylinus* cellulose; (c) cellulose by *G. xylinus* from static and agitated cultures. Adsorption isotherm is depicted in solid line and desorption is in dashed line. STP stands for standard conditions of temperature and pressure.

chains delamination may give rise to smaller, more highly crystalline cellulose nanocrystals. On the other hand, differences are observed in the structure of bacterial cellulose crystals produced in different culture conditions. In agitated culture, the crystallinity and crystallite size of the cellulose pellicles are found to be smaller than pellicles formed in static culture, which is consistent with previous report that a comparable smaller crystallinity and crystallite size were observed in agitated culture as compared to static culture by the *G. xylinus* strain NQ-5 (Czaja, Romanovicz, & Brown, 2004).

3.2. Validation of N_2 adsorption for quantifying cellulose surface area

Avicel PH101, commercial microcrystalline cellulose, was initially used to test the validity and accuracy of the surface area measurement by N_2 adsorption. Previous results showed a range of 1.3–2.2 m^2/g (Ardizzone et al., 1999; Burns et al., 1989; Fan et al., 1981; Sinitsyn, Gusakov, & Vlasenko, 1991), due to minor variations of the Avicel samples purchased, our result of 2.4 ± 0.7 m^2/g was considered to be acceptable.

3.3. N_2 adsorption–desorption isotherms and pore size distributions (PSDs)

CNWs produced by acid treatments have received much attention due to their high surface area and unique physical and mechanical properties. To study the effects of acid hydrolysis and different origins on the pore structure of cellulose, typical N_2 adsorption–desorption isotherms at 77 K for all the cellulose samples from different acid treatments and origins are shown in Fig. 1 (Supplementary data). Corresponding pore size distributions (PSDs) were calculated using the BJH method and are shown in Fig. 2. Accordingly, the calculated BET specific surface area, total meso- and macropore (1.7–300 nm) area (A_{BJH}), total meso- and macropore volume (V_{BJH}), average meso- and macropore width (D_{BJH}) and micropore (0.4–1.7 nm) volume (V_{HK}) of cellulose samples are summarized in Table 2. Generally, these N_2 isotherms show a type IV adsorption isotherm behavior with hysteresis loop, which is accompanied by capillary condensation in porous cellulose (IUPAC classification). The geometry of each porous cellulose sample can be predicted based on the shape of the hysteresis loop. According to IUPAC classification, the N_2 adsorption isotherm of untreated cotton CF11 reveals a type H3 hysteresis loop (Fig. 1a) in which the adsorption branch is steep at saturation pressure while the desorption branch is steep at intermediate relative pressure. The adsorption branch rises gradually until $P/P_0 = 0.9$, and then sharply ascends over $P/P_0 = 0.9$, and does not reach stable status even at $P/P_0 = 1$, showing that N_2 vapor confined in the pores of cellulose CF11condenses at a relative pressure lower than its saturation pressure. This type H3 hysteresis loop is usually observed with aggregates of plate-like particles giving rise to slit-shaped pores (Lowell, Shields, Thomas, & Thommes, 2004). Therefore, it is predicted that slit pores exist in cotton fiber CF11 between parallel bundles of cellulose elementary fibrils. After acid hydrolysis, the isotherms of CNWs produced by H_2SO_4 and HCl hydrolysis are compared with untreated CF11, as shown in Fig. 1a. In general, both HCl and H_2SO_4 generated CNWs have significantly increased N_2 adsorptions and wider hysteresis loops than CF11, indicating that acid hydrolysis increases the surface area and porosity. Since CNWs exhibit higher crystallinity in comparison to CF11 (Table 1), it is not likely that the increased surface area comes from the formation of more amorphous regions in cellulose. Therefore, it is hypothesized that this occurs because of the increase of external surface area as the size of the cellulose particle decreases, as well as new pore generation during acid treatments. According to the Kelvin equation (Gregg & Sing, 1982) with an assumption of cylindrical/slit pore model to describe the filling behavior in individual pores, there is a correlation between pore radius (r) and pore condensation pressure (P/P_0),

$$\ln\left(\frac{P}{P_0}\right) = -\frac{2\gamma\upsilon}{rRT}$$

where P is the pressure under which N_2 in a pore of radius (r) condenses, P_0 is the saturation pressure for N_2, γ is the surface tension of liquid N_2, υ is the molar volume of the condensed liquid N_2, R is the gas constant and T is the temperature. Condensation will happen at lower P/P_0 in small pores than in large pores, which means the hysteresis loop will start at lower P/P_0 for small pores. Our results suggest that CF11 has larger pores than H_2SO_4/HCl generated CNWs because the hysteresis loop of CF11 starts at a higher P/P_0 (0.65 vs. 0.4 for H_2SO_4/HCl generated CNWs). This is also demonstrated by the PSDs shown in Fig. 2a and b in which a major peak around 100 nm is observed in CF11. It is predicted that these macropores must exist between aggregates of fibrils since they disappear after acid treatments when the aggregates are disrupted and no longer joined, as suggested by the shift of the major peak to smaller sized pores in PSDs of CNWs.

Specifically, the hysteresis loops of H_2SO_4 generated CNWs (both upper and lower fractions) are of type H4, in which the adsorption branch is steep at saturation pressure, and desorption branch is sloping. This type H4 hysteresis loop is always associated with a heterogeneous assembly of capillaries with wide bodies and narrow necks (Allen, 1997). After H_2SO_4 hydrolysis, the hysteresis loops shifted from type H3 to H4, which suggests that H_2SO_4 hydrolysis may open up disordered regions within the bundle of elementary fibrils and thus make double tapered capillaries (where the pore becomes wider at the center) from slit-like pores. Alternatively, a slit-like pore may become wedge-shaped where the pore widens as it penetrates into the bundle, where continued hydrolysis has eliminated amorphous cellulose contained inside.

Interestingly, H_2SO_4 generated CNWs where the different fractions of the CNW suspension exhibit varied N_2 adsorption behaviors. An earlier study on ordered mesoporous silica showed that the shape and the width of hysteresis loop depended on pore radius/PSD at a given temperature (Thommes, Koehn, & Froeba, 2002). It is suggested that the width of the hysteresis loop increases with increased pore size and/or PSD. In our case, increased N_2 adsorption and wider hysteresis loop of the lower fraction of H_2SO_4 treated CNWs as compared to the upper fraction are observed. Combined with the PSD result from Fig. 2a and b, which suggests a similar pore size of the upper and lower fractions of H_2SO_4 treated CNWs, it is likely that the wider hysteresis loop of the lower fraction of CNWs results from broad PSD. In addition, larger aggregates from incomplete hydrolysis exist in the lower fraction but not in the upper fraction of the CNWs. These larger aggregates contain intact bundles of elementary fibrils in which some porous regions are still retained. On the other hand, PSDs from Fig. 2a and b also suggest that some small pores ~1.7 nm are generated in the upper fraction which might be explained by hydrolysis of amorphous cellulose between elementary fibrils. Preston and Cronshaw (1958) have speculated that an elementary cellulose fibril contains an amorphous outer shell, which would presumably be susceptible to acid hydrolysis. Alternatively, these small pores may arise due to the delamination of the cellulose sheets on the surface and ends of the CNWs by acid hydrolysis, as discussed in more detail in Section 3.5.

Different from H_2SO_4 generated CNWs, CNWs made from HCl hydrolysis exhibit varied hysteresis loops from different fractions of the CNW suspension. As it is shown in Fig. 1a, for the upper fraction, there is a high adsorption at low relative pressure ($P/P_0 < 0.4$), indicating the existence of large amount of micropores (0.4–1.7 nm) in the HCl hydrolyzed CNWs obtained from the upper fraction. Additionally, due to a large number of small mesopores of 1.7–2 nm

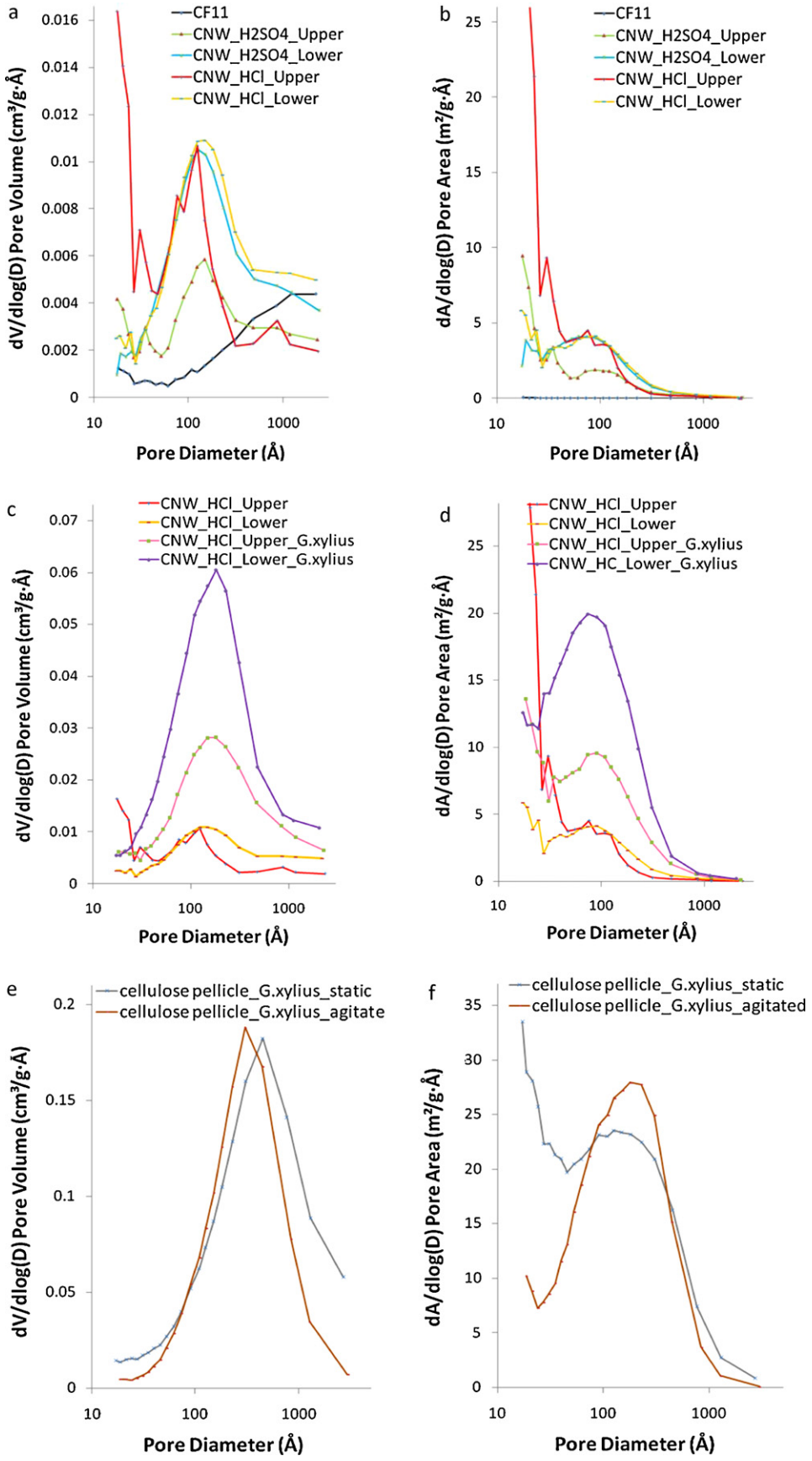

Fig. 2. BJH PSDs from N_2 adsorption isotherms. PSDs are plotted as pore volume per unit pore width ($cm^3/g\,Å$) and pore area per unit pore width ($m^2/g\,Å$), respectively. (a, b) CNWs generated by H_2SO_4 and HCl hydrolysis (plant origin); (c, d) plant cotton and bacterial CNWs generated by HCl hydrolysis; (e, f) bacterial cellulose produced from static and agitated cultures.

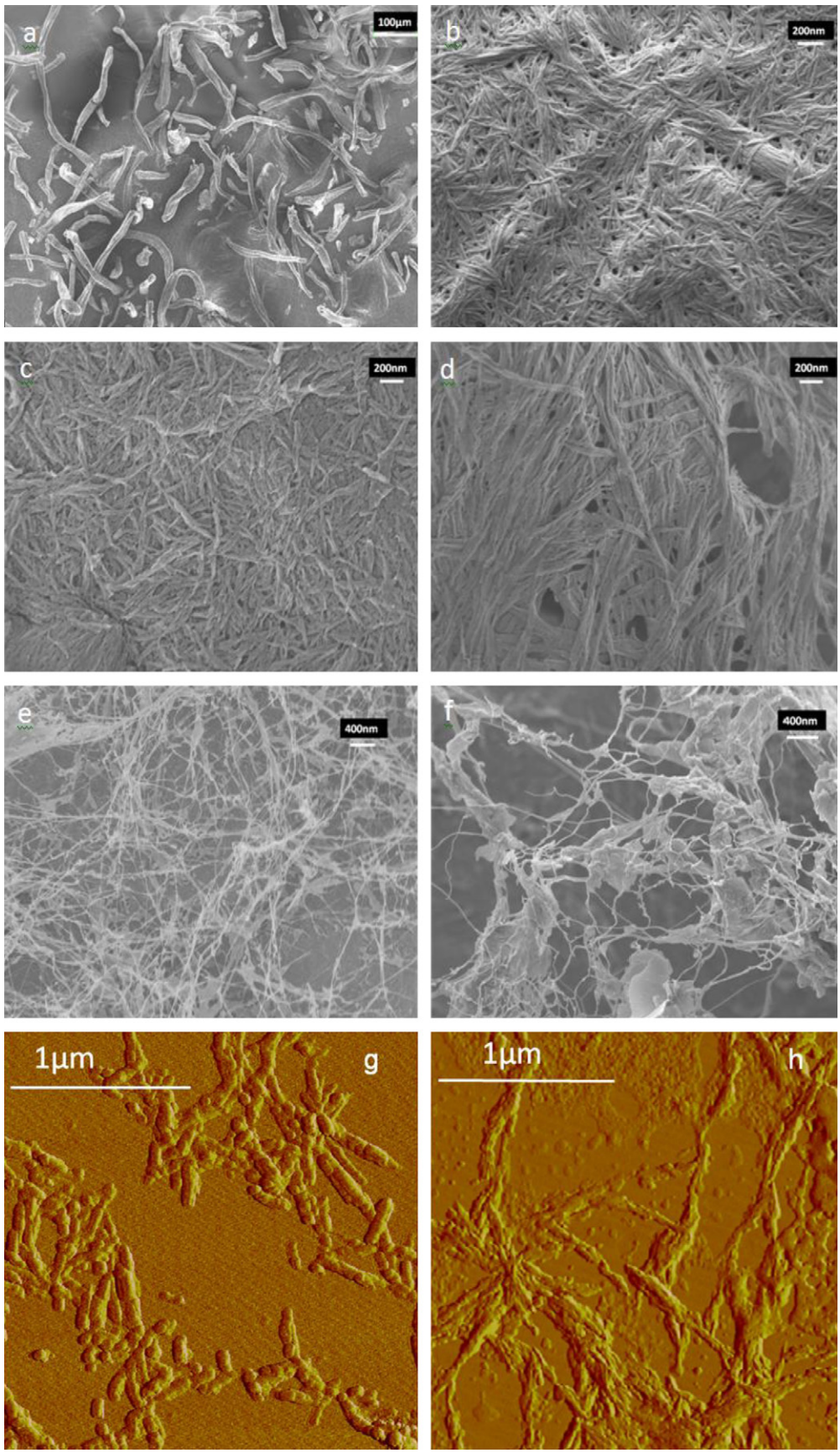

Fig. 3. FESEM and AFM images of cellulose produced under different conditions: (a) cotton CF11; (b) CNWs generated from cotton CF11 by H_2SO_4 hydrolysis; (c) CNWs generated from cotton CF11 by HCl hydrolysis; (d) CNWs produced from *G. xylinus* ATCC 700178 cellulose by HCl hydrolysis; (e) cellulose from *G. xylinus* ATCC 700178 produced statically; (f) cellulose from *G. xylinus* ATCC 700178 produced during agitation. Scale bars are shown in the figures. Cellulose samples were freeze-dried as powders (a–d) or films (e, f), fixed onto an aluminum slab with two-sided adhesive carbon tape, and sputter-coated with gold (thickness ~ 1 nm) for FESEM observation. (g) AFM phase image of cotton CNWs produced by H_2SO_4 hydrolysis; (h) AFM phase image of cotton CNWs produced by HCl hydrolysis.

Table 2
Specific surface area, macro-, meso- and microporosity of cellulose samples by BET, BJH and HK methods.

Sample	Origin	Treatment	BET surface (>0.4 nm)	Macro-, mesopore (1.7–300 nm)			Micropore (0.4–1.7 nm)	
			A_{BET} (m^2/g)	A_{BJH} (m^2/g)	V_{BJH} (cm^3/g)	Pore size (nm)	V_{HK} (cm^3/g)	Median pore width (nm)
CF11	Cotton	–	1.6 ± 0.2	1.3 ± 0.3	0.005 ± 0.001	11.7 ± 0.4	None	None
CNW_U1	CF11	H_2SO_4	5.1 ± 0.7	3.5 ± 0.2	0.007 ± 0.001	9.2 ± 0.0	None	None
CNW_L1	CF11	H_2SO_4	5.4 ± 1.2	5.4 ± 1.1	0.015 ± 0.002	11.5 ± 1.0	None	None
CNW_U2	CF11	HCl	16.8 ± 2.6	9.7 ± 0.6	0.014 ± 0.003	5.4 ± 0.4	0.005 ± 0.000	1.1 ± 0.0
CNW_L2	CF11	HCl	4.8 ± 0.7	4.8 ± 0.3	0.015 ± 0.002	12.6 ± 0.4	0.001 ± 0.000	1.0 ± 0.1
CNW_U3	*G. xylinus*	HCl	11.9 ± 0.2	10.9 ± 0.0	0.042 ± 0.012	12.4 ± 0.2	0.001 ± 0.000	0.8 ± 0.0
CNW_L3	*G. xylinus*	HCl	16.2 ± 2.9	17.6 ± 4.0	0.054 ± 0.010	12.4 ± 0.5	0.004 ± 0.001	0.9 ± 0.0
BC_S	*G. xylinus*	Static	39.2 ± 1.3	39.0 ± 1.9	0.220 ± 0.022	21.6 ± 0.1	0.010 ± 0.000	0.9 ± 0.1
BC_A	*G. xylinus*	Agitated	29.1 ± 0.7	27.5 ± 1.0	0.148 ± 0.011	23.9 ± 1.0	0.004 ± 0.002	0.8 ± 0.0

U, L represent the upper and lower fractions of CNW suspensions, respectively. CNW_1/2 refers to CNWs produced from plant CF11 by H_2SO_4/HCl hydrolysis; while CNW_3 refers to the CNWs produced from *G. xylinus* ATCC 700178 cellulose. BC_S and BC_A represent the bacterial cellulose produced by *G. xylinus* ATCC 700178 with static and agitated cultures. Median pore width is the pore width at which 50% of the total N_2 adsorbed into the cellulose sample. The values were obtained from at least duplicates.

generated in the upper fraction (Fig. 2a and b), the pore volumes are comparable for the upper and lower fractions of the HCl hydrolyzed CNWs (Table 2), even though a reduced major mesopore size (~10 nm) is observed in the upper in comparison to the lower fraction (~20 nm) (Fig. 2a). On the other hand, in the case of the lower fraction a type H4 hysteresis loop is observed, which is similar to H_2SO_4 generated CNWs. However, HCl hydrolyzed CNWs taken from the upper fraction appear to exhibit a combination of H2 and H4 type hysteresis loop, which may suggest a combination of both ink-bottle pores and tapered capillaries (Lowell et al., 2004). In the desorption branch, the steep decrease after a flat region for HCl hydrolyzed upper fraction of CNWs implies the existence of deeper pores, ink-bottle type pores with varying radius and/or interconnected pores, suggesting that more complete hydrolysis may result in more isolated cellulose crystals, where the amorphous cellulose is nearly completely removed. Interestingly, previous literature reporting size distributions of acid hydrolyzed cotton CNWs cited typical widths in the range of 10–20 nm, but typical crystallite sizes on the order of 5–7 nm by TEM (Elazzouzi-Hafraoui et al., 2008). This suggests that the CNWs themselves are probably bundles of elementary fibrils containing crystalline and amorphous regions. It may be possible that hydrolysis eliminates amorphous regions between elementary fibrils, as described above, and inside the bundle, which might cause pore percolation within crystal aggregates or within bundles. The elimination of amorphous regions within such a bundle could result in deeper, interconnected pores or pores which exhibit ink-bottle type geometry, resulting in a hysteresis loop which exhibits both type H2 and H4 behavior as observed in Fig. 1a, i.e., a sharp decrease ('knee'), which has been observed previously in alumina (Liu, Zhang, & Seaton, 1993). In addition, more complete hydrolysis may expose the ends of the cellulose nanocrystals. In this case, we further hypothesize that tapered capillaries would be generated as a result of the cellulose sheets composing the cellulose nanocrystal delaminating at the ends, thus producing micropores.

In general, the PSDs of CNWs generated by H_2SO_4 and HCl (plant origin) are very similar (Fig. 2a and b). It reveals that the existence of a maximum peak in the PSD is related to a large amount of mesopores sized in the range of 10–20 nm. In particular, the major mesopore sizes of CNWs are in the order of R-HCl_{upper} < R-HCl_{lower} ≈ R-H_2SO_{4upper} ≈ R-H_2SO_{4lower} (R is the pore radius of slit-like/cylindrical pore). It is noticed that both meso- and micropores are observed in the HCl produced CNWs, while only mesopores are present in H_2SO_4 treated CNWs (Table 2). Previous work suggested that sulfate groups were introduced onto the surface of CNWs by H_2SO_4 hydrolysis, while no chloride groups were present on the surface of CNWs isolated using HCl (Braun, Dorgan, & Chandler, 2008). This is in agreement with our preliminary X-ray photoelectron spectroscopy (XPS) data that sulfate is detected in H_2SO_4 isolated CNWs, whereas no Cl exists in HCl isolated CNWs (data not shown). A possible explanation for the absence of micropores in H_2SO_4 isolated CNWs is the surface functionalization by sulfate groups either close or block micropores, or prevent further acid hydrolysis on this scale.

The N_2 adsorption–desorption isotherms of HCl hydrolyzed CNWs from both plant and bacterial cellulose are also compared to determine the effect of different origins on the formation of CNWs. As shown in Fig. 1b, greater porosity is observed for CNWs produced from *G. xylinus* compared to those from cotton CF11. The major mesopore sizes (Fig. 2c and d) of HCl hydrolyzed CNWs are in the order of R-$Plant_{upper}$ < R-$Plant_{lower}$ ≈ R-$Bacterial_{upper}$ ≈ R-$Bacterial_{lower}$. The PSD peak of CNWs made from *G. xylinus* cellulose exhibits a small shift to a larger pore size, presumably caused by the different cellulose origins. Moreover, the higher porosity of CNWs produced by *G. xylinus* is in good correlation with previous results indicating that bacterial cellulose has higher porosity as measured by mercury porosimetry compared to plant cellulose (Brown, 1998). This may result from increased susceptibility of bacterial cellulose to hydrolysis, which yields a mesh-like cellulose fiber network with increased meso- and microporosity. On the other hand, more N_2 adsorption is obtained in the lower fraction of bacterial CNWs compared to the upper fraction (Fig. 1b), which suggests that the larger N_2 capacity for the lower fraction comes from larger mesoporosity as well as microporosity. Considering that bigger CNWs exist in the lower fraction resulting from incomplete hydrolysis, it is highly possible that larger mesoporosity comes from pores within larger bundle aggregrates left in the lower fraction. Such aggregrtates may also provide greater microporosity if the packing of these aggregrates is tight, where partial hydrolysis opens micropores within the aggregrates as well.

Bacterial cellulose generated by *G. xylinus* is also investigated in this study (Fig. 1c). Bacterial cellulose can be produced using static and agitated cultures. It is well known that static cultures yield gelatinous membranes on the surface of the medium, whereas fibrous suspensions or spheres are formed in agitated cultures (Chao, Ishida, Sugano, & Shoda, 2000; Hu & Catchmark, 2010; Watanabe, Tabuchi, Morinage, & Yoshinaga, 1998). Our results indicate that both static and agitated cultured cellulose display type H3 hysteresis loops corresponding to slit-like pores. Observing that the cellulose from the agitated culture exhibits a narrower hysteresis loop, it is deduced that smaller porosity exists in agitated cellulose (Sing et al., 1985), which might be explained by a more highly packed and rigid cellulose structure resulting in less porosity. The PSDs of pore volume show a similar trend that the PSD of agitated cultured cellulose shifts to smaller pore size in comparison to statically cultured cellulose (Fig. 2e). On the other hand, Fig. 2f indicates

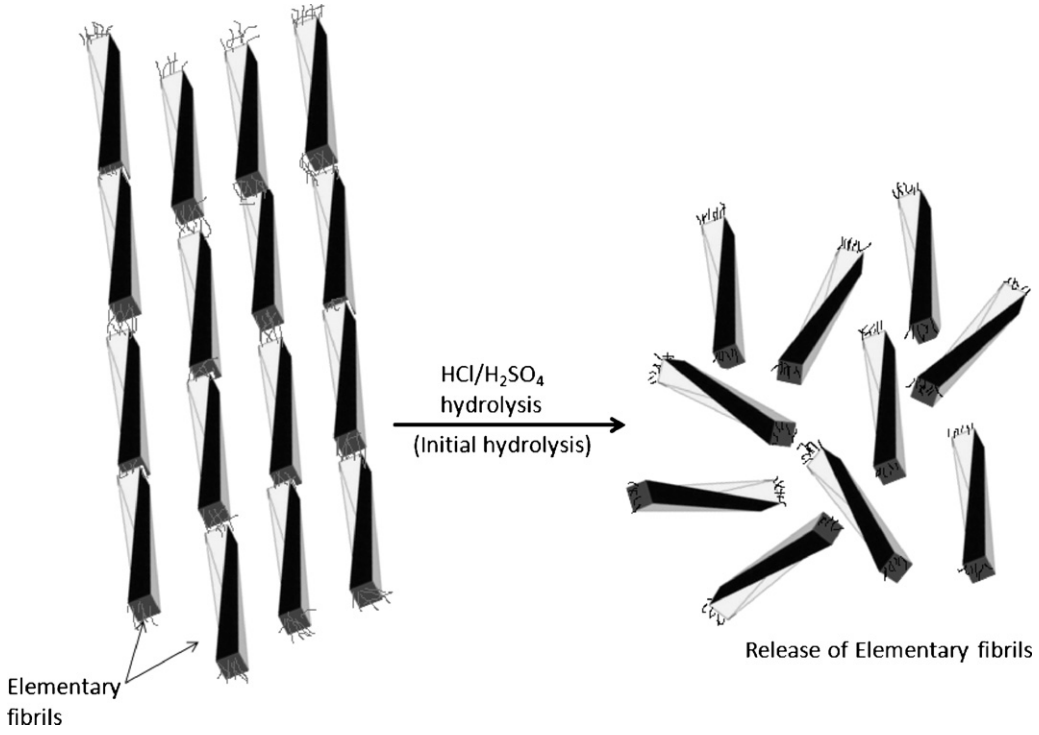

Fig. 4. A schematic illustration of the possible changes in the structure of plant cellulose microfibril subjected to HCl/H_2SO_4 treatment. The treatment causes the elimination of amorphous regions (shown at regular intervals along the length of microfibrils, although it is unknown if this is an accurate representation of plant cellulose) and the release of elementary fibrils with free ends. The grey ends represent the cross-sections of microfiber, corresponding to the (1 1 0) planes. (Twist structure is shown in cellulose microfibril, however, it is unknown whether this is continuous twist or localized twist along the microfibril.)

that statically cultured cellulose exhibits a larger number of small mesopores (1.7–3 nm), which may arise from the existence of long slits with small pore size.

3.4. Cellulose morphology characterization by FESEM and AFM

Detailed morphological characterization of different cellulose samples were carried out using FESEM and AFM. Untreated cotton CF11 fibers (Fig. 3a) show a dense structure with highly packed cellulose aggregates, resulting in low surface area and porosity (Table 2). After H_2SO_4/HCl hydrolysis, the large agglomerates of fibers disappeared and more discrete CNWs were separated and released, giving rise to needle-like structured fibers (Fig. 3b and c). Detailed observation by AFM shows that these CNWs have lengths in the range of 200–500 nm and widths (measured by the thickness of each CNW) of 7–24 nm. Both length and width are reduced by acid hydrolysis as compared to fibrous CF11. The open structure and large amount of smaller cellulose nanocrystal aggregates as well as the possible tapered/wedge-shaped capillaries formed between these aggregates might account for the increased surface area and porosity after acid hydrolysis. Fig. 3g and h are AFM images of CNWs produced by H_2SO_4 and HCl hydrolysis, respectively. CNWs produced using H_2SO_4 have an average width of 11.3 ± 2.8 nm (based on 28 measurements) and the width does not vary significantly along the length of the fiber axis. CNWs produced using HCl, however, have an average center width of 12.9 ± 4.2 nm (based on 20 measurements) and an end width of 3.4 ± 1.3 nm (based on 28 measurements). The observation that CNWs exhibiting thinner ends relative to the center regions resulting from HCl hydrolysis as compared to H_2SO_4 hydrolysis supports the hypothesis that delamination may occur to a larger extent in the HCl hydrolyzed CNWs, possibly due to more complete hydrolysis without inhibition from the introduction of sulfate groups. Fig. 3d shows bacterial CNWs also exhibit needle/rod-like structure with longer lengths (~several microns) as compared to plant CNWs, implying cellulose from different origins have varied nanocrystal structure.

As seen in Fig. 3e and f, the bacterial cellulose is generally porous with a mesh-like structure formed by entangled and interwoven elementary fibrils and bundles. The SEM image illustrates that void space dominates with the average fiber diameter of 20–30 nm. A close observation reveals that under agitation culture conditions, the cellulose produced exhibits a disordered, curved, aggregated structure, as observed previously (Czaja et al., 2004). The large surface area and porosity of the bacterial cellulose from static/agitated culture could be explained on the basis of its mesh-like, interconnected nanostructure.

3.5. Possible mechanism of acid hydrolysis on the microstructure of cellulose

Generally, the shape of native cellulose is determined by both cellulose synthases as well as by the local environment in which the cellulose is produced (Doblin et al., 2002). Depending on the biological origins, various cellulose nanocrystals are observed in this study. In higher plants, cellulose elementary fibrils are proposed to be composed of glucan chains produced by membrane rosettes (Read & Bacic, 2002), corresponding to a crystallite size for cotton cellulose (CF11) of 7.4 nm. Bacterial cellulose by *G. xylinus* is believed to form flat ribbon like microfibrils (Brown & Montezinos, 1976), a 6.2 nm crystallite is observed from the strain ATCC 700178.

Cellulose synthases create cellulose elementary fibrils, containing both crystalline and amorphous regions, which may combine into larger bundles. It has been shown that disordered amorphous regions are arranged at regular intervals along the length of Ramie cellulose microfibrils (Nishiyama et al., 2003). CNWs are formed through a degradation of amorphous regions which are more susceptible to acid hydrolysis (as shown in Fig. 4). Variation in the structure of the cellulose elementary fibrils produced in different

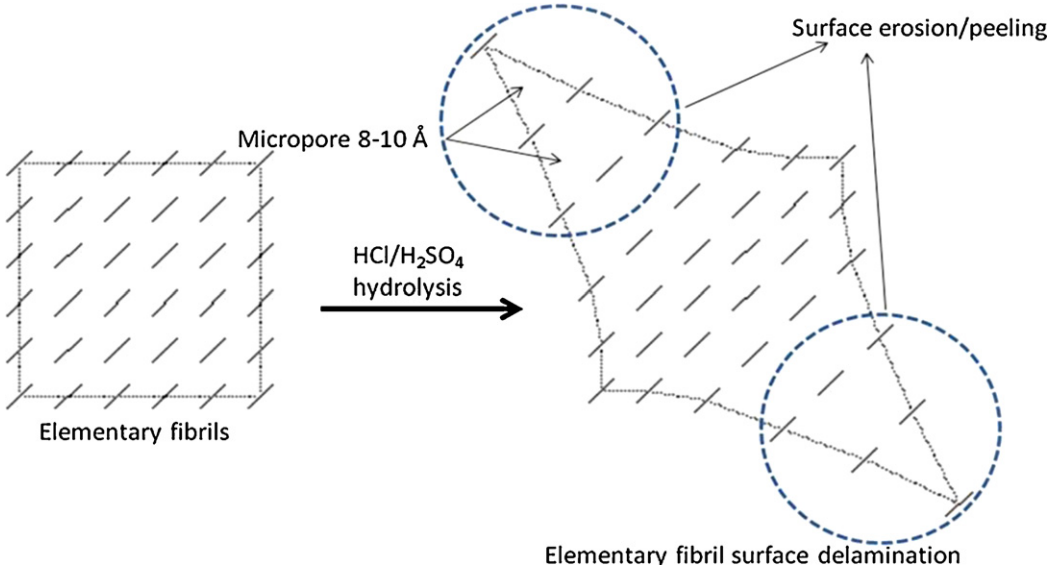

Fig. 5. A schematic illustration of a cross-section of an elementary fibril of plant cellulose. Cross-section of the elementary fibril contains 36 glucan chains and these glucan chains are indicated as straight lines. After acid hydrolysis, delamination occurs at the end external surface of CNWs producing micropores (width: ~8–10 Å).

organisms results in an associated variation in the length of CNWs (Elazzouzi-Hafraoui et al., 2008; Favier, Chanzy, & Cavaille, 1995; Habibi et al., 2010; Petersson, Kvien, & Oksman, 2007; Samir et al., 2005).

During the initial stage of hydrolysis, we hypothesize that the removal of the amorphous cellulose gives rise to unstable fibril ends, resulting in the delamination, or to say, the surface erosion/peeling of glucan sheets associated with the cellulose crystal. This delamination/surface erosion may occur at the ends and more extensively along the external surface where the terminal glucan planes exist and micropores in the range of ~0.8–1.0 nm (Table 2) may be generated at the beginning of delamination (right before the erosion) of the cellulose crystal. Delamination at the ends and external surface of the CNWs is illustrated in Fig. 5, and this is supported by crystallite width measurements using AFM. After HCl hydrolysis sharp ends of CNWs (with average width of 3.4 nm) appear compared to the center body of CNWs (with average width of 12.9 ± 4.2 nm). Delamination of the surface glucan chains has been previously suggested by Grohmann, Torget, and Himmel (1986). Additionally, this is supported by previous work suggesting that chopped, rounded microfibrils were observed after sulfuric acid hydrolysis of tunicate cellulose (Helbert, Nishiyama, Okano, & Sugiyama, 1998). In another work, there was an initial significant weight loss during acid hydrolysis which correlated with a dramatic reduction in the degree of polymerization (DP). As the hydrolysis continued, the weight loss also continued at a reduced rate, but no decrease in the DP was observed (Nishiyama et al., 2003). Based on these data, we speculate that the continued weight loss is associated with the hydrolysis of surface glucan chains starting from the ends, which is also responsible for the rounding of the ends of the cellulose fibrils observed by Helbert et al. (1998), i.e., glucans located at the edges of the fibril ends become more susceptible to hydrolysis due to delamination. This process does not significantly impact the DP of the remaining cellulose glucan chains contained in the crystal. The concept of cellulose layer delamination/erosion is also in agreement with Frey-Wyssling's observation (1954) that

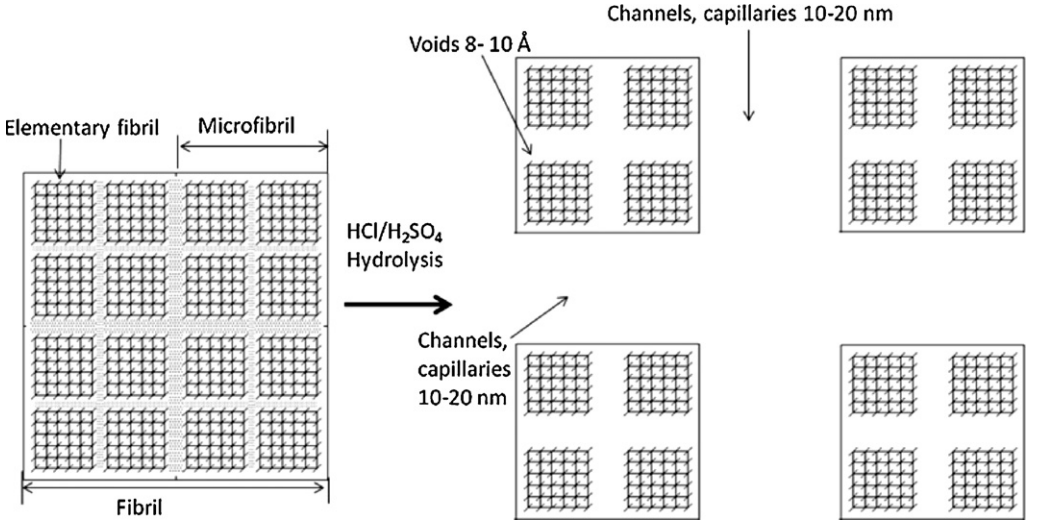

Fig. 6. Schematic illustration of pore creation during acid hydrolysis through the disruption of aggregated bundles. Cross-section of a bundle of elementary fibrils of plant cellulose (left) and a disrupted bundle where smaller bundles of four microfibrils have been separated (right) are shown. Voids (width: 8–10 Å) may be generated between elementary fibrils during acid hydrolysis. Channel and capillaries (width: 10–20 nm) may also be generated between the microfibrils during acid hydrolysis.

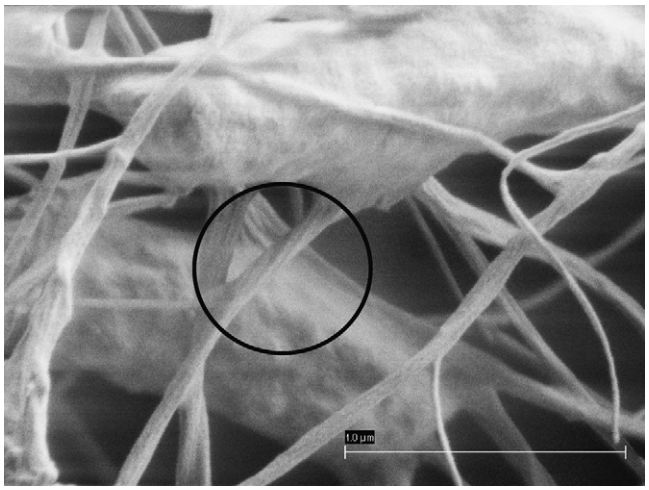

Fig. 7. FESEM image of cellulose produced by *G. xylinus* ATCC 700178 showing bundles formation. A bundle clearly showing twist is highlighted in the image. The highlighted bundle is approximately 80 nm in diameter. A 1 μm scale bar is shown in the image.

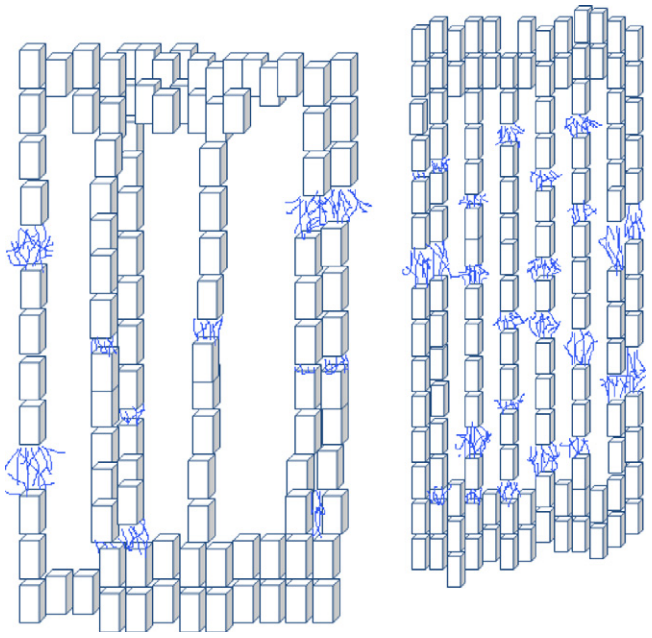

Fig. 8. Schematic diagram showing the microstructure of bacterial cellulose microfibrils produced from static (left) and agitated (right) cultures. Smaller elementary fibril crystals (depicted by blocks) and more amorphous regions are formed in agitated culture than that from static culture.

the microfibrils are laminated and easily split parallel to the (1 1 0) plane.

In addition to the creation of micropores in the range of ~0.8–1.0 nm in width through delamination of the cellulose crystal, acid hydrolysis may also generate new micropores (<1.7 nm) and mesopores (10–20 nm) in width through the separation of closely packed fibrils or bundles (Fig. 6). As noted above, size distributions of H_2SO_4 hydrolyzed cotton CNWs cited typical widths in the range of 10–20 nm, and our AFM observations show widths of 11.3 ± 2.8 nm for H_2SO_4 hydrolyzed cotton CNWs and 12.9 ± 4.2 nm for HCl hydrolyzed CNWs, but typical crystal sizes are on the order of 5–7 nm (Elazzouzi-Hafraoui et al., 2008). This suggests that the CNWs are themselves bundles of elementary fibrils containing crystalline and noncrystalline regions, where some of the noncrystalline content may exist between the crystalline regions associated with the elementary fibrils. This is also supported by a molecular model of a 36-chain elementary fibril proposed by Ding and Himmel (2006), Preston and Cronshaw (1958) and Lucia and Rojas (2009). It is suggested that the elementary fibril is a heterogeneous structure containing both a center crystalline core and layers of subcrystalline/noncrystalline surface chains. The macrofibril is formed by the aggregation of elementary fibrils. Hydrolysis of this noncrystalline content may produce deeper or interconnected pores within elementary fibril and/or tapered capillaries between bundles of elementary fibrils, and/or pores which exhibit ink-bottle type geometry, as observed in this work.

Other possible causes for new pore generation may include any strain present in the cellulose crystal or bundle which, if present, may be released once the amorphous region is removed. Bundle formation itself may impose strain on the cellulose fibrils depending upon the origin of the bundle. We have observed twisted bundle formation in cellulose produced by *G. xylinus* (Fig. 7).

Cellulose produced by *G. xylinus* ATCC 700178 possesses high surface area and porosity. The structure of bacterial cellulose also varies depending on the culture conditions. Bacterial cellulose microfibrils from agitated cultures have lower crystallinity and crystallite size as compared to cellulose produced from static cultures. It is hypothesized that this arises from different stresses imposed on the cellulose as it is being produced using these different culture methods. Higher stresses may impede crystallization resulting in smaller fibril widths, increased amorphous content and increased packing density. This is shown schematically in Fig. 8.

4. Conclusions

N_2 adsorption isotherms of cellulose samples formed by different acid treatments and from different origins were analyzed to obtain information about cellulose surface area, pore volume, pore area, and PSD. It is shown that CF11, commercial fibrous cellulose, has the smallest specific surface area and porosity. HCl and H_2SO_4 treatments result in a significant increase in surface area and porosity. Since these treatments result in reduced amorphous content, the increased surface area likely results from fibril and bundle disruption. In addition, new microporosity is observed in HCl treated cellulose, especially in the upper fraction. It is hypothesized that this new microporosity results either from the delamination of the cellulose crystal sheets when the amorphous cellulose is removed; or from the hydrolysis of amorphous cellulose in between bundles of elementary fibrils. Bacterial CNWs from *G. xylinus* show significantly increased porosity as compared to plant originated CNWs. Cellulose generated by *G. xylinus* in agitated or static culture generally shows similar pore size, however, agitated cultured cellulose exhibits smaller surface area and porosity. These findings may allow various forms of cellulose to be used more effectively in both scientific and engineering applications. Although our work shows a quantitative characterization of surface area and porosity of cellulose from different origins and treatments, more detailed information on the production of these pores and the difference of pore features from different origins and treatments needs to be elucidated in future research.

Acknowledgements

This work was funded by United State Department of Agriculture-NRI: 2007-35504-18339. We thank Dr. Magda N. Salama from the Penn State Materials Characterization Lab (MCL) for her instruction on the use of the ASAP 2020 instrument. We thank Jin Gu, Yang Hu and Lin Fang for making CNWs and *G. xylinus* cellulose pellicles. We also thank the staff of the Penn State Nanofabrication Facility, where FESEM analysis was performed. This publication was supported by the Pennsylvania

State University Materials Research Institute Nanofabrication Lab and the National Science Foundation Cooperative Agreement No. 0335765, National Nanotechnology Infrastructure Network, with Cornell University.

Appendix A. Supplementary data

Supplementary data associated with this article can be found, in the online version, at doi:10.1016/j.carbpol.2011.07.060.

References

Aggebrandt, L. G. & Samuelson, O. (1964). Penetration of water-soluble polymers into cellulose fibers. *Journal of Applied Polymer Science*, *8*(6), 2801–2812.

Allen, T. (1997). Particle size measurement. *Surface area and pore size determination* (5th ed., Vol. 2, pp. 44–108). US/London, UK: Springer/Chapman & Hall.

Araki, J., Wada, M., Kuga, S. & Okano, T. (1998). Flow properties of microcrystalline cellulose suspension prepared by acid treatment of native cellulose. *Colloids and Surfaces A: Physicochemical and Engineering Aspects*, *142*(1), 75–82.

Ardizzone, S., Dioguardi, F. S., Mussini, T., Mussini, P. R., Rondinini, S., Vercelli, B., et al. (1999). Microcrystalline cellulose powders: Structure, surface features and water sorption capacity. *Cellulose*, *6*(1), 57–69.

Attala, R. H. & Vanderhart, D. L. (1984). Native cellulose: A composite of two distinct crystalline forms. *Science*, *223*(4633), 283–285.

Barret, E. P., Joyner, L. G. & Halenda, P. H. (1951). The determination of pore volume and area distributions in porous substrates. I. Computations from nitrogen isotherms. *Journal of the American Chemical Society*, *73*(1), 373–380.

Bondeson, D., Mathew, A. & Oksman, K. (2006). Optimization of the isolation of nanocrystals from microcrystalline cellulose by acid hydrolysis. *Cellulose*, *13*(2), 171–180.

Braun, B., Dorgan, J. R. & Chandler, J. P. (2008). Cellulose nanowhiskers. Theory and application of light scattering from polydisperse spheroids in the Rayleigh–Gans–Debye regime. *Biomacromolecules*, *9*(4), 1255–1263.

Brown, R. M., Jr. (1998). Microbial cellulose: A new resource for wood, paper, textiles, food and specialty products. Position Paper, http://www. botany. utexas.edu/facstaff/facpages/mbrown.

Brown, R. M., Jr. & Montezinos, D. (1976). Cellulose microfibrils: Visualization of biosynthetic and orienting complexes in association with the plasma membrane. *Proceedings of the National Academy of Sciences of the United States of America*, *73*(1), 143–147.

Brunauer, S., Emmett, P. H. & Teller, E. (1938). Adsorption of gases in multimolecular layers. *Journal of the American Chemical Society*, *60*(2), 309–319.

Burns, D. S., Ooshima, H. & Converse, A. O. (1989). Surface area of pretreated lignocellulosics as a function of the extent of enzymatic hydrolysis. *Applied Biochemistry and Biotechnology*, *20*(1), 79–94.

Chao, Y., Ishida, T., Sugano, Y. & Shoda, M. (2000). Bacterial cellulose production by *Acetobacter xylinum* in a 50-L internal-loop airlift reactor. *Biotechnology and Bioengineering*, *68*(3), 345–352.

Czaja, W., Romanovicz, D. & Brown, R. M. (2004). Structural investigations of microbial cellulose produced in stationary and agitated culture. *Cellulose*, *11*(3), 403–411.

Delmer, D. P. & Amor, Y. (1995). Cellulose biosynthesis. *Plant Cell*, *7*(7), 987–1000.

De Souza Lima, M. M. & Borsali, R. (2004). Rodlike cellulose microcrystals: Structure, properties, and applications. *Macromolecular Rapid Communications*, *25*(7), 771–787.

Ding, S. Y. & Himmel, M. E. (2006). The maize primary cell wall microfibril: A new model derived from direct visualization. *Journal of Agricultural and Food Chemistry*, *54*(3), 597–606.

Doblin, M. S., Kurek, I., Jacob-Wilk, D. & Delmer, D. P. (2002). Cellulose biosynthesis in plants: From genes to rosettes. *Plant and Cell Physiology*, *43*(12), 1407–1420.

Elazzouzi-Hafraoui, S., Nishiyama, Y., Putaux, J. L., Heux, L., Dubreuil, F. & Rochas, C. (2008). The shape and size distribution of crystalline nanoparticles prepared by acid hydrolysis of native cellulose. *Biomacromolecules*, *9*(1), 57–65.

Fan, L. T., Lee, Y. H. & Beardmore, D. R. (1981). The influence of major structural features of cellulose on rate of enzymatic hydrolysis. *Biotechnology and Bioengineering*, *23*(2), 419–424.

Favier, V., Chanzy, H. & Cavaille, J. Y. (1995). Polymer nanocomposites reinforced by cellulose whiskers. *Macromolecules*, *28*(18), 6365–6367.

Frey-Wyssling, A. (1954). The fine structure of cellulose microfibrils. *Science (Washington, DC, U.S.)*, *119*(3081), 80–82.

Galle, C. (2001). Effect of drying on cement-based materials pore structure as identified by mercury intrusion porosity. A comparative study between oven-, vacuum-, and freeze-drying. *Cement and Concrete Research*, *31*, 1467–1477.

Gama, F. M., Teixeira, J. A. & Mota, M. (1994). Cellulose morphology and enzymatic reactivity: A modified solute exclusion technique. *Biotechnology and Bioengineering*, *43*(5), 381–387.

Gregg, S. J. & Sing, K. S. W. (1982). *Adsorption, surface area and porosity* (p. 303).(2nd ed.). London: Academic Press.

Grohmann, K., Torget, R. & Himmel, M. (1986). Dilute acid pretreatment of biomass at high solids concentrations. *Biotechnology and Bioengineering Symposium*, *15*, 59–80.

Habibi, Y., Lucia, L. A. & Rojas, O. J. (2010). Cellulose nanocrystals: Chemistry, self-assembly, and applications. *Chemical Reviews*, *110*(6), 3479–3500.

Helbert, W., Nishiyama, Y., Okano, T. & Sugiyama, J. (1998). Molecular imaging of *Halocynthia papillosa* cellulose. *Journal of Structural Biology*, *124*, 42–50.

Hestrin, S. & Schramm, M. (1954). Synthesis of cellulose by *Acetobacter xylinum*. *Biochemical Journal*, *58*, 345–352.

Horvath, G. & Kawazoe, K. (1983). Method for calculation of effective pore size distribution in molecular sieve carbon. *Journal of Chemical Engineering of Japan*, *16*(6), 470–475.

Hu, Y. & Catchmark, J. M. (2010). Formation and characterization of spherelike bacterial cellulose particles produced by *Acetobacter xylinum* JCM 9730 strain. *Biomacromolecules*, *11*(7), 1727–1734.

Ioelovitch, M. (1992). On the supermolecular structure of native and isolated cellulose samples. *Acta Polymerica*, *43*(2), 110–113.

Klemm, D., Heublein, B., Fink, H. P. & Bohn, A. (2005). Cellulose: Fascinating biopolymer and sustainable raw material. *Angewandte Chemie International Edition*, *44*(22), 3358–3393.

Krieger, J. (1990). Bacterial cellulose near commercialization. *Chemical and Engineering News*, *68*(21), 35–37.

Krokida, M. K., Karathanos, V. T. & Maroulis, Z. B. (1998). Effect of freeze-drying conditions on shrinkage and porosity of dehydrated agricultural products. *Journal of Food Engineering*, *35*(4), 369–380.

Kulshreshtha, A. K. & Dweltz, N. E. (1973). Paracrystalline lattice disorder in cellulose I. Reappraisal of the application of 2-phase hypothesis to analysis of powder X-ray diffractograms of native and hydrolyzed cellulosic materials. *Journal of Polymer Science Part B: Polymer Physics*, *11*(3), 487–497.

Liu, H. L., Zhang, L. & Seaton, N. A. (1993). Sorption hysteresis as a probe of pore structure. *Langmuir*, *9*, 2576–2582.

Lowell, S. & Shields, J. E. (1991). *Powder surface area and porosity* (p. 250).(3rd ed.). London: Chapman and Hall.

Lowell, S., Shields, J. E., Thomas, M. A. & Thommes, M. (2004). *Characterization of porous solids and powders: Surface area, pore size and density* (pp. 101–126). Dordrecht, Netherlands: Kluwer Academic Publishers.

Lucia, L. A., & Rojas, O. J. (Eds.). (2009). Front matter. In *The nanoscience and technology of renewable biomaterials*. Chichester, UK: John Wiley & Sons, Ltd.

Marchessault, R. H., Morehead, F. F. & Koch, M. J. (1961). Some hydrodynamic properties of neutral suspensions of cellulose crystallites as related to size and shape. *Journal of Colloid Science*, *16*(4), 327–344.

Marchessault, R. H., Morehead, F. F. & Walter, N. M. (1959). Liquid crystal systems from fibrillar polysaccharides. *Nature*, *184*(4686), 632–633.

Morosoff, N. (1974). Never dried cotton fibres. III. Crystallinity and crystallite size. *Journal of Applied Polymer Science*, *18*(6), 1837–1854.

Nishiyama, Y., Kim, U. J., Kim, D. Y., Katsumata, K. S., May, R. P. & Langan, P. (2003). Periodic disorder along ramie cellulose microfibrils. *Biomacromolecules*, *4*(4), 1013–1017.

Papadopoulos, A. N., Hill, C. A. S., Gkaraveli, A., Ntalos, G. A. & Karastergiou, S. P. (2003). Bamboo chips (*Bambusa vulgaris*) as an alternative lignocellulosic raw material for particleboard manufacture. *European Journal of Wood and Wood Products*, *62*(1), 36–39.

Petersson, L., Kvien, I. & Oksman, K. (2007). Structure and thermal properties of poly (lactic acid)/cellulose whiskers nanocomposite materials. *Composites Science and Technology*, *67*(11-12), 2535–2544.

Preston, R. D. & Cronshaw, J. (1958). Constitution of the fibrillar and non-fibrillar components of the walls of *Valonia ventricosa*. *Nature*, *181*(4604), 248–250.

Ratti, C. (2001). Hot air and freeze-drying of high-value foods: A review. *Journal of Food Engineering*, *49*, 311–319.

Read, S. M. & Bacic, T. (2002). Prime time for cellulose. *Science (Washington, DC, U.S.)*, *295*(5552), 59–60.

Rouquerol, F., Rouquerol, J. & Sing, K. (1999). *Adsorption by powders and porous solids, principles, methodology and applications*. San Diego, CA: Academic Press.

Sakairi, N., Asano, H., Ogawa, M., Nishi, N. & Tokura, S. (1998). A method for direct harvest of bacterial cellulose filaments during continuous cultivation of *Acetobacter xylinum*. *Carbohydrate Polymers*, *35*(3–4), 233–237.

Samir, M. A. S. A., Alloin, F. & Dufresne, A. (2005). Review of recent research into cellulosic whiskers, their properties and their application in nanocomposite field. *Biomacromolecules*, *6*(2), 612–626.

Sing, K. S. W., Everett, D. H., Haul, R. A. W., Moscou, L., Pierotti, R. A., Rouquerol, J., et al. (1985). Reporting physisorption data for gas/solid systems. *Pure and Applied Chemistry*, *57*(4), 603–619.

Sinitsyn, A. P., Gusakov, A. V. & Vlasenko, E. Y. (1991). Effect of structural and physic-chemical features of cellulosic substrates on the efficiency of enzymatic hydrolysis. *Applied Biochemistry and Biotechnology*, *30*(1), 43–58.

Stone, J. E., Scallan, A. M., Donefer, E. & Ahlgren, E. (1969). Digestibility as a simple function of a molecule of similar size to a cellulase enzyme. Cellulases and their applications. *Advances in Chemistry Series*, *95*, 219–241.

Thode, E. F., Swanson, J. W. & Becher, J. J. (1958). Nitrogen adsorption on solvent-exchanged wood cellulose fibers: Indications of "total" surface area and pore size distribution. *Journal of Physical Chemistry*, *62*(9), 1036–1039.

Thommes, M., Koehn, R. & Froeba, M. (2002). Sorption and pore condensation behavior of pure fluids in mesoporous MCM-48 silica, MCM-41 silica, SBA-15 silica and controlled-pore glass at temperatures above and below the bulk triple point. *Applied Surface Science*, *196*, 239–249.

Thompson, D. N., Chen, H. C. & Grethlein, H. E. (1992). Comparison of pretreatment methods on the basis of available surface area. *Bioresource Technology*, *39*(2), 155–163.

Watanabe, K., Tabuchi, M., Morinage, Y. & Yoshinaga, F. (1998). Structural features and properties of bacterial cellulose produced in agitated culture. *Cellulose*, *5*, 187–200.

Wong, K. K. Y., Deverell, K. F., Mackie, K. L., Clark, T. A. & Donaldson, L. A. (1988). The relationship between fiber porosity and cellulose digestibility in steam-exploded *Pinus radiate*. *Biotechnology and Bioengineering*, *31*(5), 447–456.

Zhang, L. N., Xi, Q., Mo, Z. S. & Jin, X. G. (2003). *Current researching methods on polymer physics* (pp. 194–195). Wuhan College Press.